

Article

Excited-State Dynamics of Carbazole and *tert*-Butyl-Carbazole in Organic Solvents

Konstantin Moritz Knötig [†] , Domenic Gust [†], Thomas Lenzer  and Kawon Oum ^{*†} 

Physical Chemistry 2, Department Chemistry and Biology, Faculty IV, School of Science and Technology, University of Siegen, Adolf-Reichwein-Str. 2, 57076 Siegen, Germany; konstantin.knoetig@uni-siegen.de (K.M.K.); domenic.gust@uni-siegen.de (D.G.); lenzer@chemie.uni-siegen.de (T.L.)

* Correspondence: oum@chemie.uni-siegen.de

[†] These authors contributed equally to this work.

Abstract: Carbazole-based molecular units are ubiquitous in organic optoelectronic materials; however, the excited-state relaxation of these compounds is still underexplored. Here, we provide a detailed investigation of carbazole (Cz) and 3,6-di-*tert*-butylcarbazole (*t*-Bu-Cz) in organic solvents using femtosecond and nanosecond UV–Vis–NIR transient absorption spectroscopy, as well as time-resolved fluorescence experiments upon photoexcitation in the deep-UV range. The initially prepared S_x singlet state has a (sub-)picosecond lifetime and decays to the S_1 state by internal conversion (IC). The S_1 state exhibits absorption peaks at 350, 600 and 1100 nm and has a lifetime of 13–15 ns, which is weakly dependent on the solvent. Energy transfer from vibrationally hot S_1 molecules (S_1^*) to the surrounding solvent molecules takes place with a time constant of 8–20 ps. The T_1 triplet state is populated by intersystem crossing (ISC) from S_1 with a typical quantum yield of 51–56% and shows a lifetime which is typically in the few microseconds regime. The S_1 and T_1 states of both carbazole compounds in solution are strongly quenched by O_2 . Two-photon excitation leads to the formation of a small amount of the respective radical cation. The influence of the *tert*-butyl substituents on the photophysics is relatively weak and mainly reflects itself in a small increase in the Stokes shift. The results provide important photophysical information for the interpretation of carbazole relaxation in more complex environments.

Keywords: carbazole; excited-state dynamics; deep-UV ultrafast laser spectroscopy; triplet formation



Citation: Knötig, K.M.; Gust, D.; Lenzer, T.; Oum, K. Excited-State Dynamics of Carbazole and *tert*-Butyl-Carbazole in Organic Solvents. *Photochem* **2024**, *4*, 163–178. <https://doi.org/10.3390/photochem4020010>

Academic Editors: Marcelo Guzman, Vincenzo Vaiano and Rui Fausto

Received: 31 December 2023

Revised: 20 March 2024

Accepted: 28 March 2024

Published: 30 March 2024



Copyright: © 2024 by the authors. Licensee MDPI, Basel, Switzerland. This article is an open access article distributed under the terms and conditions of the Creative Commons Attribution (CC BY) license (<https://creativecommons.org/licenses/by/4.0/>).

1. Introduction

Carbazole-based compounds represent one of the core components in the field of organic optoelectronic devices. They are used as molecular building blocks, oligomers, dendrimers or polymers and exhibit several distinct advantages, such as low cost of the starting materials, facile access to functionalization at the nitrogen atom and easy linkage through the carbazole backbone [1–5]. In particular, they show beneficial electronic and photophysical properties with respect to organic light-emitting diode (OLED) applications [6], as they feature high-energy S_1 and T_1 states, which are essential for their functions either as host materials or as molecular electron donor moieties in efficient emitters based on donor–acceptor concepts featuring thermally activated delayed fluorescence (TADF) [7–10].

A comprehensive understanding of the function of such optoelectronic materials requires a good knowledge regarding the excited-state dynamics of the parent compound carbazole and its ring-substituted analogs under “isolated” conditions, because in more dense environments, such as thin films, the intramolecular carbazole chromophore relaxation is in competition with processes such as singlet–singlet, singlet–triplet and triplet–triplet annihilation, as well as slow vibrational cooling of the thin film, which lead to a complex spectral and kinetic behavior [11–15]. The majority of the previous studies on Cz have focused on basic photophysical properties, such as absorption and fluorescence spectra,

which have been characterized in considerable detail [6]. For instance, the steady-state absorption, fluorescence and phosphorescence spectra of carbazole have been reported in solution and the gas phase [16–21]. In addition, triplet–triplet absorption spectra have been provided [22,23]. Moreover, the quenching of the Cz T₁ triplet state, intramolecular excimer formation, hydrogen-bonding interactions and hydrogen transfer reactions from carbazole derivatives to bases, such as pyridine, have been studied in detail [24–31].

In contrast, time-resolved studies of the photoinduced dynamics of these compounds have been less frequently reported and focused on the transient fluorescence of the S₁ state. Lifetimes in the range of 7–15 ns have been reported for Cz in different organic solvents [17,26,29,32,33]. Transient broadband absorption measurements mainly involved *N*-alkylated carbazole derivatives [15,34–36]. Bayda-Smykaj et al. reported Vis–NIR transient absorption spectra for Cz in acetonitrile up to 2.6 ns, but no femtosecond transient absorption (fs-TA) experiments for wavelengths below 450 nm, and also no detailed kinetic analysis of the TA spectra were provided [34]. Hiyoshi et al. employed picosecond and nanosecond transient absorption (ns-TA) spectroscopy covering the spectral range of 380–810 nm mainly to explore the relevance of photodeprotonation and photoionization processes of carbazole and *N*-ethylcarbazole in organic solvents induced by two-photon excitation. However, they provided only transient spectra at selected time delays and did not perform an in-depth kinetic analysis [37].

Therefore, the goal of the current work is to investigate in detail the excited-state dynamics of carbazole in the organic solvents *n*-heptane, tetrahydrofuran (THF) and acetonitrile upon photoexcitation in the wavelength range of 260–273 nm. In addition, the closely related 3,6-di-*tert*-butylcarbazole is studied in the same solvents because of the importance of such 3,6-dialkyl-substituted chromophores as electron donor moieties in donor–acceptor TADF compounds [38,39]. A comprehensive characterization of the photoinduced relaxation mechanism of these carbazole derivatives is achieved by a combination of fs-TA and ns-TA spectroscopy, as well as time-correlated single photon counting (TCSPC).

2. Materials and Methods

2.1. Chemicals Used and Preparation of Solutions

Carbazole (TCI Deutschland, Eschborn, Germany, high purity), 3,6-di-*tert*-butylcarbazole (TCI Deutschland, >98.0%), *n*-heptane (Merck, Darmstadt, Germany, Uvasol, ≥99.9%), tetrahydrofuran (THF, Merck, Uvasol, ≥99.9%) and acetonitrile (ACN, Merck, Uvasol, ≥99.9%) were used without further purification. For the preparation of the solutions, a defined amount of Cz or *t*-Bu-Cz was freshly dissolved in the organic solvent of interest. The organic solvents were placed in a septum-sealed vial which was pierced by two stainless steel hollow needles, one used for bubbling nitrogen gas (Messer Industriegase GmbH, 4.6, Bad Soden, Germany) through the solution (duration: 90 min) and the other one used as outlet. Cz or *t*-Bu-Cz were dissolved in the nitrogen-saturated solvent of interest and the colorless solution was then passed through a PTFE filter (pore size 0.45 μm). All sample-handling steps were carried out in a glove box under a nitrogen atmosphere in order to minimize unwanted contact with air.

2.2. Steady-State Absorption and Fluorescence

The steady-state absorption measurements were performed by using a double-beam spectrophotometer (Varian Inc., Palo Alto, CA, USA, Cary 5000). Prior to the experiments, a baseline without a sample was recorded and subtracted afterwards. A quartz cuvette (Hellma, Müllheim, Germany) containing the nitrogen-flushed pure solvent served as a reference. The steady-state emission spectra were measured by using a fluorescence spectrophotometer (Agilent, Santa Clara, CA, USA, Cary Eclipse). The slit width was adjusted to 5 nm for excitation and emission, and the emission spectra were recorded with a resolution of 1 nm. The emission spectra were corrected for the wavelength-dependent sensitivity of the detection system. Steady-state experiments were performed in quartz cuvettes with path lengths of 1 or 10 mm (Hellma).

2.3. Time-Correlated Single Photon Counting

The experimental TCSPC arrangement, originally reported by Morgenroth et al. [40], is described below. Briefly, a pulsed (500 ps full width at half maximum (FWHM)) UV-LED with a center wavelength of 273 nm served as the excitation source. The excitation pulses were vertically polarized (0°) by a wire-grid linear polarizer prior to sample excitation. The resulting sample emission was collected by a quartz lens positioned at an angle of 90° with respect to the pulsed LED beam and then passed another wire-grid linear polarizer, which was set at the magic angle of 54.7° to avoid any contributions of orientational relaxation of the chromophores to the emission signal. A part of the emission spectrum was selected by a bandpass filter (center wavelength 370 nm, FWHM 10 nm) and detected by a hybrid-alkali photodetector. Fluorescence decays were recorded at a repetition frequency of 1 MHz. The fluorescence decays were fitted by a single exponential function with a small constant offset using an iterative reconvolution procedure applying an instrument response function, which was obtained from the LED scattering signal of a diluted suspension of colloidal silica nanoparticles in water. Concentrations of Cz and *t*-Bu-Cz in the TCSPC and steady-state fluorescence experiments were in the range of $6\text{--}11 \times 10^{-6} \text{ mol L}^{-1}$. The nitrogen-bubbled Cz and *t*-Bu-Cz solutions were placed under nitrogen in an airtight cuvette.

2.4. Femtosecond and Nanosecond Transient Absorption Spectroscopy

Broadband transient absorption experiments with a time resolution of ca. 80 fs covering delay times up to 1500 ps were carried out at a repetition frequency of 920 Hz on two setups dedicated to measurements in the UV-Vis [41] and NIR ranges [42]. They are both based on the pump-supercontinuum probe (PSCP) method [43]. Excitation was performed at 260 nm by an OPA system with a repetition frequency of 460 Hz and a pulse energy in the range of 300–390 nJ, corresponding to a fluence of $1.1\text{--}1.5 \text{ mJ cm}^{-2}$. Measurements up to a delay time of 10 μs were carried out by interfacing the UV-Vis setup with a Q-switched Nd:YAG microlaser, as described previously [44], using its fourth harmonic at 266 nm (FWHM ca. 420 ps) for excitation, with similar fluences as for the femtosecond experiments. Solutions of Cz or *t*-Bu-Cz ($T = 296 \text{ K}$) were placed under nitrogen in an airtight quartz cuvette with a path length of 1 mm, with typical concentrations in the range of $1\text{--}5 \times 10^{-4} \text{ mol L}^{-1}$. During the measurements, the cuvette was constantly moved in a plane perpendicular to the propagation axis of the probe beam to minimize any photochemical decomposition and also local heating effects of the solutions that could occur by repeated laser excitation of the same sample volume.

3. Results

3.1. Steady-State Absorption and Emission of Carbazole and 3,6-Di-Tert-Butyl-Carbazole

The steady-state absorption and fluorescence spectra of Cz and *t*-Bu-Cz were investigated in the organic solvents *n*-heptane, THF and acetonitrile at 296 K (Figure 1). Characteristic parameters are summarized in Table 1. The spectra for Cz (panels a–c) show three main bands: The structured absorption band in the wavelength range of 300–340 nm corresponds to the short-axis polarized $S_0 \rightarrow S_1$ transition. The S_1 state has A_1 symmetry and is a L_a state according to Platt's notation [19,21,28,45,46]. The $S_0 \rightarrow S_2$ transition at about 290 nm is long-axis polarized, and the S_2 state is of B_2 symmetry [28,45]. The absorption bands below 270 nm arise from a combination of several electronic bands with B_2 and A_1 symmetry [45], which we will denote by the collective notation S_x later on. For Cz in acetonitrile, we determined the absolute absorption coefficient for the longest-wavelength peak in the absorption spectrum at 334 nm as $3900 \text{ L mol}^{-1} \text{ cm}^{-1}$. This value is expected to be only weakly dependent on the solvent.

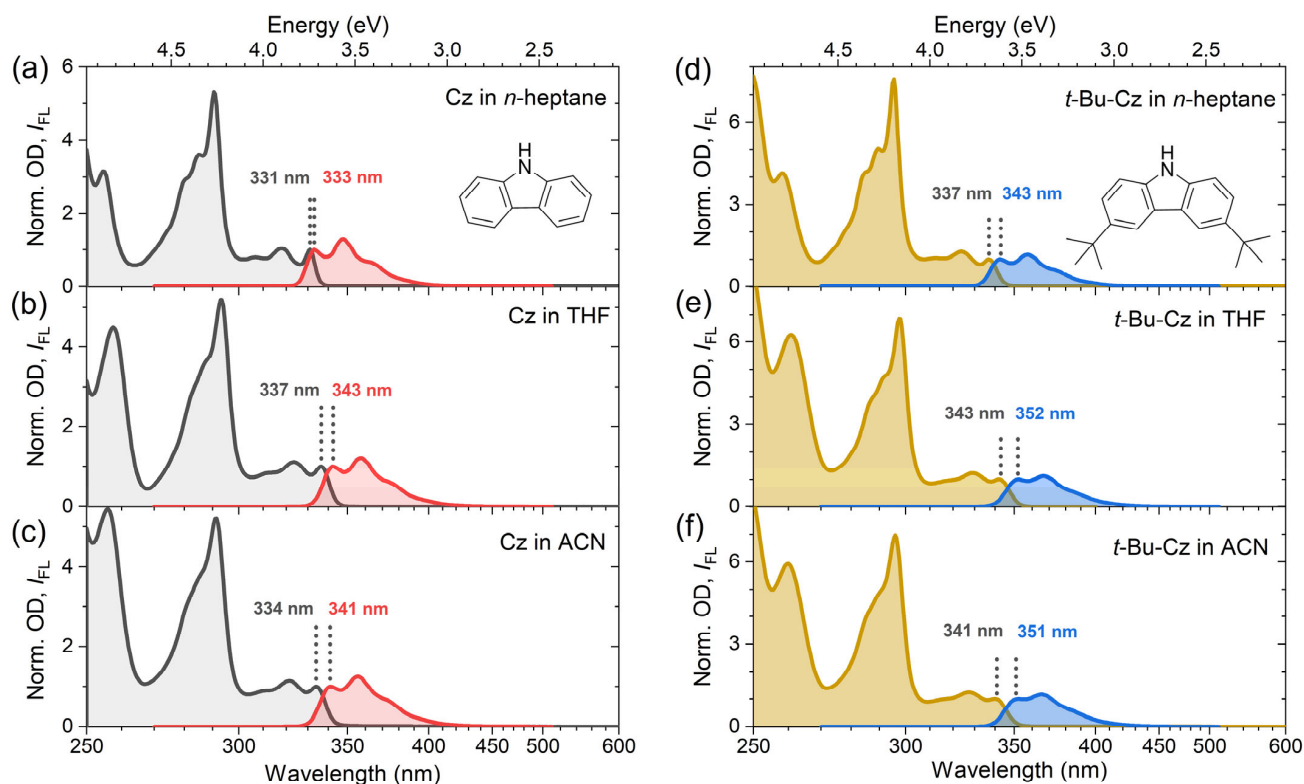


Figure 1. (a–c) Normalized steady-state absorption spectra (black) and normalized fluorescence spectra (red) of carbazole (Cz) in *n*-heptane, THF and acetonitrile, respectively. (d–f) Normalized steady-state absorption spectra (brown) and normalized fluorescence spectra (blue) of 3,6-di-*tert*-butylcarbazole (*t*-Bu-Cz) in the same solvents. The 0–0 transitions of the absorption and emission spectra are indicated by black dotted lines and labeled by the respective wavelength values. Molecular structures of Cz and *t*-Bu-Cz are provided in panels (a,d), respectively.

For all of the three solvents, the emission bands are observed in the wavelength range of 330–420 nm. They resemble the mirror image of the respective S_1 absorption band and show substantial spectral overlap with the corresponding absorption spectra. The solvatochromic behavior of Cz was analyzed by fitting the structured electronic bands to a sum of Gaussian functions, which provided the positions of the 0–0 transition in absorption and emission as well as the Stokes shift (Table 1). The spectral positions showed only a weak solvent dependence, with a variation of less than 8 nm. The Stokes shifts of Cz were estimated from the difference between the 0–0 transitions of the absorption and emission bands. They are very small and appear to increase slightly with solvent polarity, as identified by the solvent polarity parameter Δf (which is based on the known values for the refractive index n and the dielectric constant ϵ) [47,48]. They range from 193 cm^{-1} in *n*-heptane to 614 cm^{-1} in acetonitrile, which corresponds to only 2–7 nm in this wavelength range. This suggests that only minor structural changes between the S_0 and S_1 states occur. The finding is supported by previous experiments of Pratt and co-workers using rotationally resolved electronic spectroscopy of isolated Cz molecules in a molecular beam. They found only a slight decrease in the rotational constants of Cz upon excitation from the S_0 to the S_1 state. This was attributed to minor ring expansions, which are typical of π – π^* transitions [21]. Moreover, the planarity of the π -system is conserved in the S_1 state [21]. We note that correlations of the Stokes shift with other parameters, such as the Lorenz–Lorentz function $R(n)$ or the solvent viscosity η , did not provide any systematic trends.

Table 1. Summary of steady-state spectroscopic properties of carbazole (Cz) and 3,6-di-*tert*-butylcarbazole (*t*-Bu-Cz) in organic solvents at 296 K.

Molecule	Solvent	Δf ¹	$\lambda_{\text{abs}}^{0-0}$ (nm)	$\lambda_{\text{fl}}^{0-0}$ (nm)	$\Delta\lambda_{\text{Stokes}}^{0-0}$ (nm)	$\Delta\tilde{\nu}_{\text{Stokes}}^{0-0}$ (cm ⁻¹)
Cz	<i>n</i> -Heptane	≈0	331	333	2	193
	THF	0.44	337	343	6	525
	Acetonitrile	0.71	334	341	7	614
<i>t</i> -Bu-Cz	<i>n</i> -Heptane	≈0	337	343	6	519
	THF	0.44	343	352	9	745
	Acetonitrile	0.71	341	351	10	835

¹ The solvent polarity function was estimated as $\Delta f = R(\epsilon) - R(n)$, where $R(\epsilon) = (\epsilon - 1)/(\epsilon + 2)$ and $R(n) = (n^2 - 1)/(n^2 + 2)$, with the dielectric constant ϵ and the refractive index n of the respective solvent and the value for *n*-heptane being essentially identical to that of *n*-hexane [47,48].

The panels d–f of Figure 1 display the corresponding results for *t*-Bu-Cz in the same solvents. The shape of the absorption and emission bands is similar to those of Cz. However, all spectra are systematically shifted to larger wavelengths (by about 6 and 10 nm, for absorption and emission, respectively), and this red shift can be attributed to the larger polarizability of *t*-Bu-Cz. In addition, the resulting Stokes shifts are slightly larger (in the range of 519–835 cm⁻¹, corresponding to 6–10 nm) compared with Cz and also increase with solvent polarity. It therefore appears as if the two *tert*-butyl substituents only have a minor impact on the steady-state spectroscopic properties of the carbazole chromophore in solution.

3.2. Transient Absorption Studies and TCSPC Experiments of Carbazole in Organic Solvents

Femtosecond and nanosecond transient absorption spectroscopy as well as time-correlated single photon counting measurements were performed for Cz in three organic solvents at 296 K. Figures 2–4 summarize the spectral data and the kinetic analysis of the ultrafast excited-state dynamics of Cz in *n*-heptane, THF and acetonitrile, respectively. Figure 5 provides a sketch of the proposed kinetic mechanism, and Table 2 summarizes time constants from the kinetic fits.

The ultrafast excited-state dynamics of carbazole upon photoexcitation at 260 nm were recorded using fs-TA from the sub-picosecond time range up to 1.45 ns over the probe wavelength range of 260–1600 nm. We note that around a zero delay time, there was a pronounced coherent signal from the solvent itself, especially in the deep-UV region. In Figures 2–4, the spectral development is presented as a contour plot in panel a and also for selected time windows in panels b and c. We start with the dynamics of Cz in *n*-heptane (Figure 2). The initially prepared S_x state quickly relaxes to the S_1 state via ultrafast internal conversion with a time constant $\tau_x = k_x^{-1}$ of ca. 0.7 ps. In panels b and c, a ground state bleach feature (GSB, $S_0 \rightarrow S_2$) at 290 nm and characteristic $S_1 \rightarrow S_n$ ESA bands with peaks at 350, 600 and 1100 nm are clearly visible. In particular, the two S_1 ESA bands at 600 and 1100 nm show a distinct spectral narrowing on the time scale up to 50 ps (panel b), which we assign to collisional energy transfer (CET) from vibrationally hot carbazole molecules (S_1^*) to the surrounding “cold” solvent molecules. The detailed kinetic analysis provides a time constant $\tau_{\text{CET}} = k_{\text{CET}}^{-1}$ of 19 ps for this spectral evolution, see panel d for the multiexponential fits to the time traces at various probe wavelengths. Such dynamics have been frequently observed for other vibrationally excited molecules in organic solvents, such as, for example, azulene, anthracene derivatives, *trans*-stilbene and carotenoids [49–53].

The kinetic traces of the fs-TA experiments in panel d do not noticeably decay. Therefore, additional experiments using ns-TA spectroscopy and time-resolved emission were performed to elucidate the fate of the S_1 state on longer time scales (panels e–h). As shown in panel h, the fluorescence decay curve of the S_1 state of carbazole in *n*-heptane at 296 K obtained from TCSPC using a bandpass filter with a center wavelength of 370 nm (FWHM

of 10 nm) is well described by a monoexponential fit with a small constant offset, resulting in a total S_1 lifetime $\tau_1 = k_1^{-1}$ of 14.7 ns, which was also used as the long component in the fit of the fs-TA kinetics in panel d. The ns-TA spectroscopy experiments using excitation at 266 nm provide further insight into the decay dynamics of the S_1 state; see the contour plot in panel e and the nanosecond transient absorption spectra for selected times in panels f and g. At early times (1–12 ns, panel f), the ESA bands of the S_1 state near 350 nm and 600 nm dominate. At ca. 330 nm, the structured UV ESA band shows clear indications for an overlapping $S_0 \rightarrow S_1$ GSB ($0 \rightarrow 0'$ transition) and $S_1 \rightarrow S_0$ stimulated emission (SE) feature ($0' \rightarrow 0$ transition) of the S_1 state, as can be seen by comparison with the inverted steady-state absorption spectrum (magenta) and the steady-state stimulated emission spectrum (cyan). Similar spectral features located at 316 nm ($0 \rightarrow 1'$) and 347 nm ($0' \rightarrow 1$) can be again assigned to vibronic structure in the GSB and SE bands. The small amplitude of these features underscores that the absorption coefficient of the $S_0 \rightarrow S_1$ band (about $3900 \text{ L mol}^{-1} \text{ cm}^{-1}$ at 334 nm, as mentioned above) is much smaller than that of the overlapping, strongly allowed $S_1 \rightarrow S_n$ ESA band, which has a value of about $20,000 \text{ L mol}^{-1} \text{ cm}^{-1}$ at 620 nm [54].

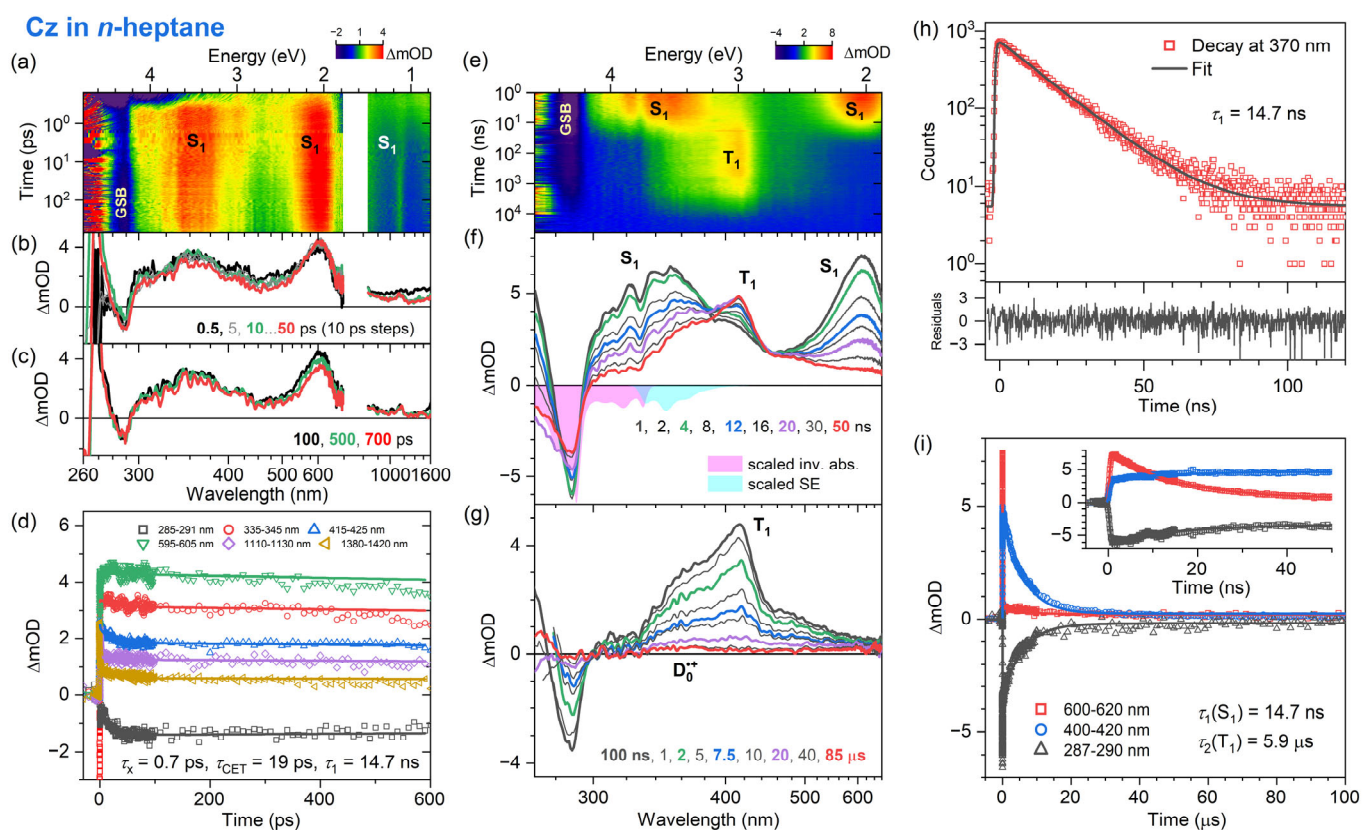


Figure 2. Time-resolved optical spectroscopy of carbazole (Cz) in *n*-heptane at 296 K ($\lambda_{\text{pump}} = 260 \text{ nm}$ for fs-TA, $\lambda_{\text{pump}} = 266 \text{ nm}$ for ns-TA and $\lambda_{\text{pump}} = 273 \text{ nm}$ for TCSPC). (a) fs-TA spectra for the time range up to 700 ps shown as a contour plot. (b,c) fs-TA spectra for selected time windows. (d) Kinetic traces and fits at selected wavelengths obtained from the fs-TA data. (e) Contour plot of ns-TA spectra. (f,g) ns-TA spectra at selected times, including the inverted and scaled steady-state absorption spectrum (magenta) and the steady-state stimulated emission spectrum (cyan). (h) TCSPC signal (red symbols) obtained using a bandpass filter centered at 370 nm, including a monoexponential fit with a small constant offset (black) and fit residuals (lower panel). (i) Kinetic traces and fits of the ns-TA data for the wavelength ranges 600–620 nm, 400–420 nm and 287–290 nm, where S_1 , T_1 and ground-state bleaching, respectively, have dominant contributions (cf. panels (f,g)). The time constants τ_1 and τ_2 represent the total lifetimes of the S_1 state and the T_1 state, respectively. The constant offset arises from the long-lived carbazole radical cation ($D_0^{*\bullet}$, cf. panel (g)).

On even longer time scales (panel g), the S_1 ESA bands have disappeared and a new ESA band near 420 nm has built up, which is assigned to the T_1 state [22,23,37,54]. It decays on the time scale of several microseconds. Kinetic traces extracted from the nanosecond transient absorption data are compared in panel i of Figure 2 for three wavelength ranges: 600–620 nm (red, predominantly decay of S_1), 400–420 nm (blue, mainly formation and decay of T_1) and 286–290 nm (black, mainly GSB and thus recovery of S_0). The kinetic analysis in panel i demonstrates that the time traces in the nanosecond transient absorption signals are well reproduced by biexponential fits, with a time constant of 14.7 ns for the formation of T_1 via intersystem crossing (ISC) from S_1 , and a time constant of 5.9 μ s for the lifetime of T_1 ($\tau_2 = k_2^{-1}$). Note that the time constant of 14.7 ns obtained from the fit to the ns-TA experiments agrees with the S_1 lifetime found in the TCSPC measurements in panel h. In addition, a long-lived, weakly absorbing species with a broad spectrum was observed (340–660 nm, cf. panel g at 85 μ s). We propose that this spectral feature arises from the $Cz^{\bullet+}$ radical cation (doublet ground state, $D_0^{\bullet+}$). First of all, it strongly resembles the flat steady-state absorption spectrum of $Cz^{\bullet+}$ reported by Shida et al., which was obtained by exposing Cz in an organic matrix at 77 K to γ radiation [55]. Secondly, the vertical ionization energy of Cz was previously reported as 7.68 eV (161 nm) [56]. Therefore, resonant two-photon ionization of Cz via the S_x state by our pump laser pulse at 266 nm will be energetically feasible. The radical cation lives longer than the time window covered in the ns-TA experiments, and thus only a lower limit can be given for its lifetime τ_{RCat} .

An accurate determination of the quantum yield for the formation of T_1 from S_1 is not possible; however, an estimate may be provided based on the known absorption coefficients of the S_1 ESA band of carbazole at 620 nm ($20,000 \text{ L mol}^{-1} \text{ cm}^{-1}$), the T_1 ESA band at 420 nm ($14,500 \text{ L mol}^{-1} \text{ cm}^{-1}$) [54] and our ns-TA spectra at 1 ns (predominantly S_1 ESA) and about 50 ns (predominantly T_1 ESA), as shown in panel f of Figure 2, resulting in a triplet quantum yield of about 55% (Table 2). This value is in very good agreement with previous estimates in the range of 45–60% by the groups of Huber and Ware [17,26]. Therefore, the individual contributions to τ_1 in the mechanism of Figure 5 are $\tau_{1,ISC} = \tau_1 / \Phi_{ISC} \approx 26.7 \text{ ns}$ and $\tau_{1,IC+FI} = \tau_1 / \Phi_{IC+FI} \approx 32.7 \text{ ns}$ where $\tau_1 = (\tau_{1,ISC}^{-1} + \tau_{1,IC+FI}^{-1})^{-1}$ (i.e., $k_1 = k_{1,ISC} + k_{1,IC+FI}$). Regarding the quantum yields for the parallel fluorescence and IC channels from S_1 , Ware, Huber and co-workers estimate values of $\Phi_{FI} \approx 40\%$ and $\Phi_{IC} \leq 15\%$, respectively [17,26].

Comparable dynamic behavior is observed for the electronic relaxation of carbazole in mid-polar THF and polar acetonitrile, as demonstrated in Figures 3 and 4, respectively. The fs-TA experiments provide ESA band shapes (panels a–c) and decay kinetics (panel d) which are similar to Cz in *n*-heptane: The lifetime τ_x of the initially prepared S_x state in the two solvents is ultrashort (about 0.2 ps), and the time constant τ_{CET} for collisional energy transfer to the solvent is 19 and 21 ps in THF and acetonitrile, respectively (Table 2). The S_1 lifetimes obtained from TCSPC (panel h) are 13.6 ns in THF and 14.3 ns in acetonitrile (Table 2). The S_1 lifetime of carbazole is therefore only weakly dependent on the solvent. This is understandable because Cz exhibits only a small change in dipole moment upon photoexcitation, from 1.9 D in the ground state to 3.1 D in the S_1 state [57].

The ns-TA spectra (panels e–g) show the decay of the two S_1 ESA bands with peaks at 350 and 600 nm and the subsequent formation of the T_1 state with a band centered at about 420 nm. The decay of the T_1 state occurs with a time constant of 3.4 μ s in THF and 10.3 μ s in acetonitrile. As for Cz in *n*-heptane, a small-amplitude, long-lived absorption signal arises from the $Cz^{\bullet+}$ radical cation. Therefore, also in these two solvents, the excited-state relaxation processes of Cz are well described by the kinetic scheme provided in Figure 5. The time constants and triplet quantum yields are summarized in Table 2.

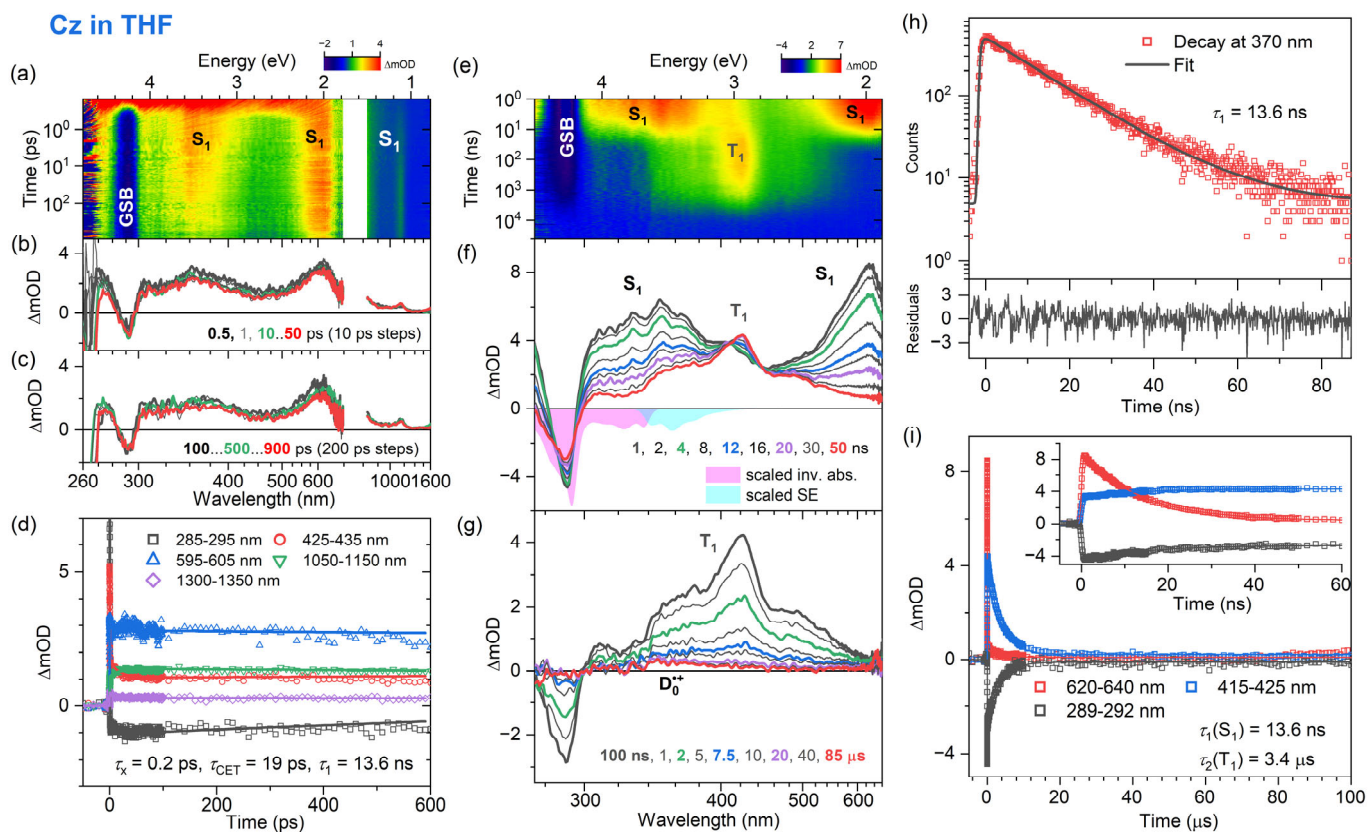


Figure 3. Same as Figure 2 but for carbazole in THF.

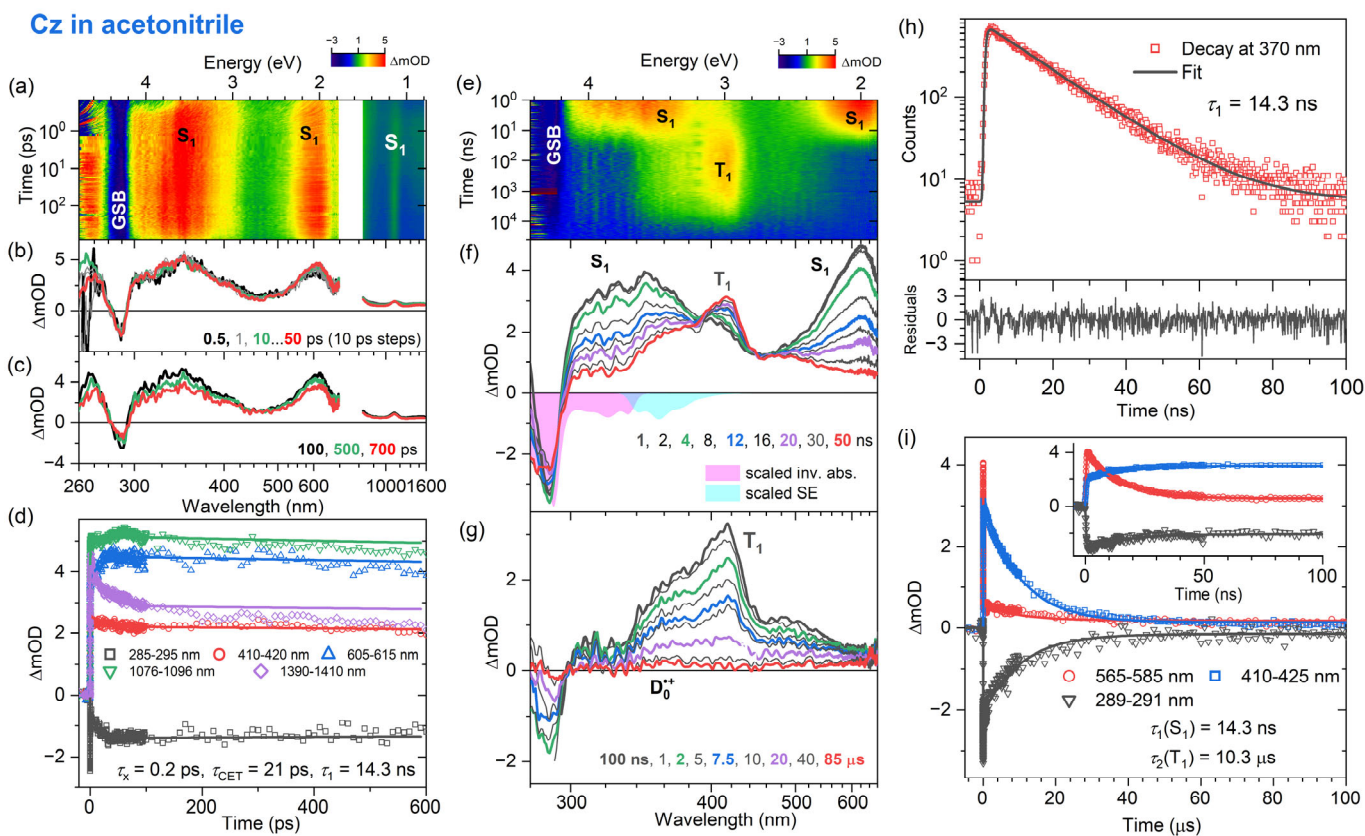


Figure 4. Same as Figure 2 but for carbazole in acetonitrile.

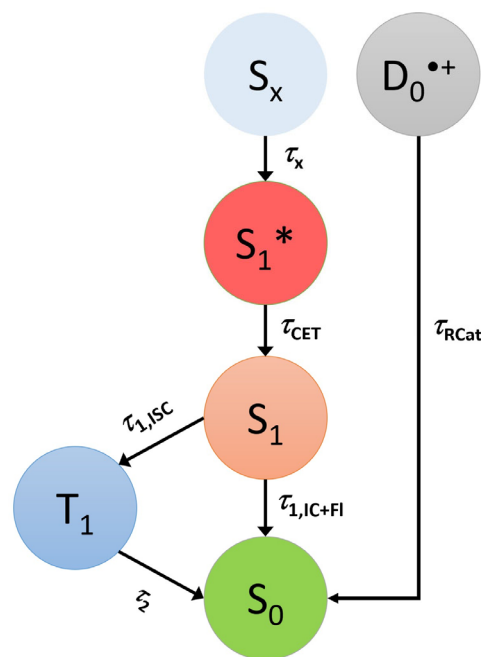


Figure 5. Kinetic scheme describing the different pathways for the relaxation of Cz and *t*-Bu-Cz upon photoexcitation by a laser. The S_x state is prepared by one-photon excitation, whereas the $D_0^{\bullet+}$ radical cation is likely generated by a small fraction of two-photon excitation with subsequent ionization.

Table 2. Summary of time constants of carbazole (Cz) in organic solvents at 296 K obtained from femtosecond and nanosecond transient absorption as well as TCSPC experiments.

Cz	fs-TA		TCSPC		ns-TA	
	τ_x	τ_{CET}	τ_1 (S_1)	τ_2 (T_1)	Φ (T_1)	τ_{RCat}
<i>n</i> -Heptane	0.7 ps	19 ps	14.7 ns	5.9 μs	55%	>50 μs
THF	0.2 ps	19 ps	13.6 ns	3.4 μs	51%	>50 μs
Acetonitrile	0.2 ps	21 ps	14.3 ns	10.3 μs	56%	>50 μs

3.3. Transient Absorption and TCSPC Experiments for 3,6-Di-Tert-Butyl Carbazole in Organic Solvents

The influence of additional alkyl substituents at the aromatic ring system on the excited-state dynamics was explored by investigating the Cz derivative 3,6-di-*tert*-butylcarbazole in *n*-heptane, THF and acetonitrile using fs-TA, ns-TA and TCSPC measurements. The experimental results are summarized in Figures 6–8. Characteristic parameters from the kinetic fitting procedure are compiled in Table 3.

The fs-TA experiments for *t*-Bu-Cz were performed for excitation at 260 nm, and an overview of the dynamics is provided by the contour plots in panel a of each figure. The IC process from the initially populated S_x state to the S_1 state is ultrafast in all cases ($\tau_x = 1.3$, 0.04 and 0.3 ps for *n*-hexane, THF and acetonitrile, respectively). The S_1 state shows the typical ESA bands also observed for Cz, with peaks at 350, 600 and 1100 nm (panels b and c). In addition, a spectral narrowing of the S_1 ESA bands at 600 and 1100 nm is observed, which is assigned to the transfer of vibrational excess energy from vibrationally hot (S_1^*) *t*-Bu-Cz to the solvents, with $\tau_{\text{CET}} = 8.9$, 16 and 16 ps for *n*-hexane, THF and acetonitrile, respectively (panel b). On longer time scales (panel c), the kinetics do not decay visibly. This is consistent with the results of the TCSPC experiments (panel h, $\lambda_{\text{pump}} = 273$ nm), which reveal a slow monoexponential decay of the S_1 state with time constants of 15.0, 12.7 and 14.1 ns in *n*-heptane, THF and acetonitrile, respectively. This behavior is also consistent with our findings for Cz and suggests quite a weak intramolecular charge transfer (ICT) character of the S_1 state.

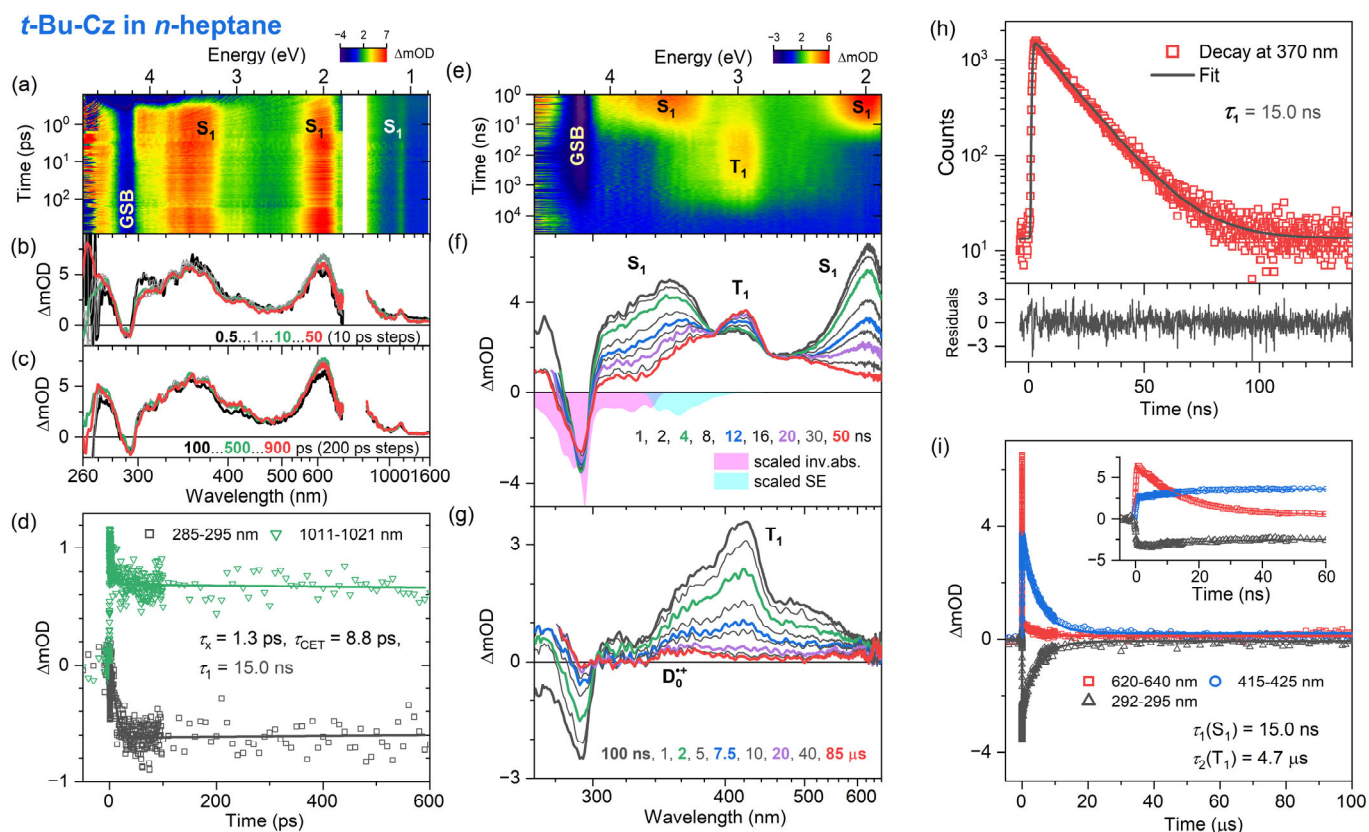


Figure 6. Time-resolved optical spectroscopy of 3,6-di-*tert*-butylcarbazole (*t*-Bu-Cz) in *n*-heptane at 296 K ($\lambda_{\text{pump}} = 260$ nm for fs-TA, $\lambda_{\text{pump}} = 266$ nm for ns-TA and $\lambda_{\text{pump}} = 273$ nm for TCSPC). Arrangement of the panels as in Figure 2.

Table 3. Summary of time constants of 3,6-di-*tert*-butylcarbazole (*t*-Bu-Cz) in organic solvents at 296 K obtained from femtosecond and nanosecond transient absorption as well as TCSPC experiments.

<i>t</i> -Bu-Cz	fs-TA		TCSPC		ns-TA	
	τ_x	τ_{CET}	τ_1 (S_1)	τ_2 (T_1)	Φ (T_1)	τ_{RCat}
<i>n</i> -Heptane	1.3 ps	8.9 ps	15.0 ns	4.7 μ s	53%	>50 μ s
THF	0.04 ps	16 ps	12.7 ns	4.2 μ s	36%	>50 μ s
Acetonitrile	0.3 ps	16 ps	14.1 ns	7.5 μ s	54%	>50 μ s

The excited-state dynamics of *t*-Bu-Cz on longer time scales were investigated using ns-TA experiments over the time range of 1 ns–100 μ s (panels e–g, $\lambda_{\text{pump}} = 266$ nm). The S_1 spectrum with the two distinct peaks at 350 and 600 nm is replaced on longer time scales by the spectrum of the T_1 state, which has a peak at 420 nm and a pronounced shoulder toward 600 nm (panel g). The lifetime of the T_1 state is 4.7, 4.2 and 7.5 μ s in *n*-heptane, THF and acetonitrile, respectively (panel i and Table 3). An estimate of the quantum yield for T_1 formation based on the known S_1 and T_1 absorption coefficients of Cz [54] and the transient spectra in panel f of Figures 6–8 provides triplet quantum yields of 55%, 36% and 54%, respectively. The shape of the T_1 spectrum depends only weakly on the solvent. Similar to Cz, we observe the formation of a small fraction of a long-lived broadly absorbing species in all solvents (340–660 nm, see panel g of Figures 6–8 at 85 μ s). This spectral feature is assigned to the *t*-Bu-Cz $^{\bullet+}$ radical cation ($D_0^{\bullet+}$), which is generated via resonant two-photon ionization by the 266 nm pump laser pulse, as explained for Cz above. Because of its long lifetime, we can only provide a lower limit for the time constant τ_{RCat} of the *t*-Bu-Cz $^{\bullet+}$ species, as in the case of Cz $^{\bullet+}$.

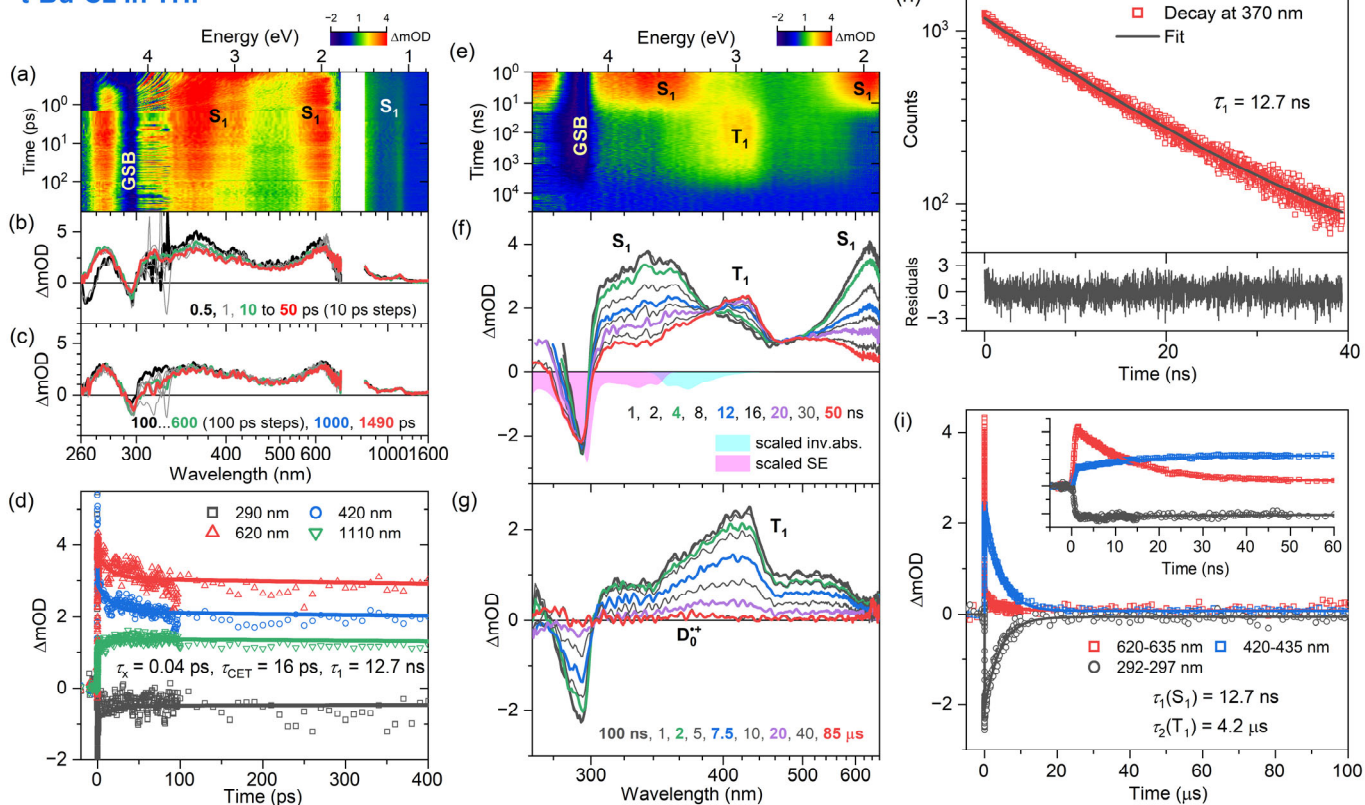
***t*-Bu-Cz in THF**

Figure 7. Same as Figure 6 but for the solvent THF.

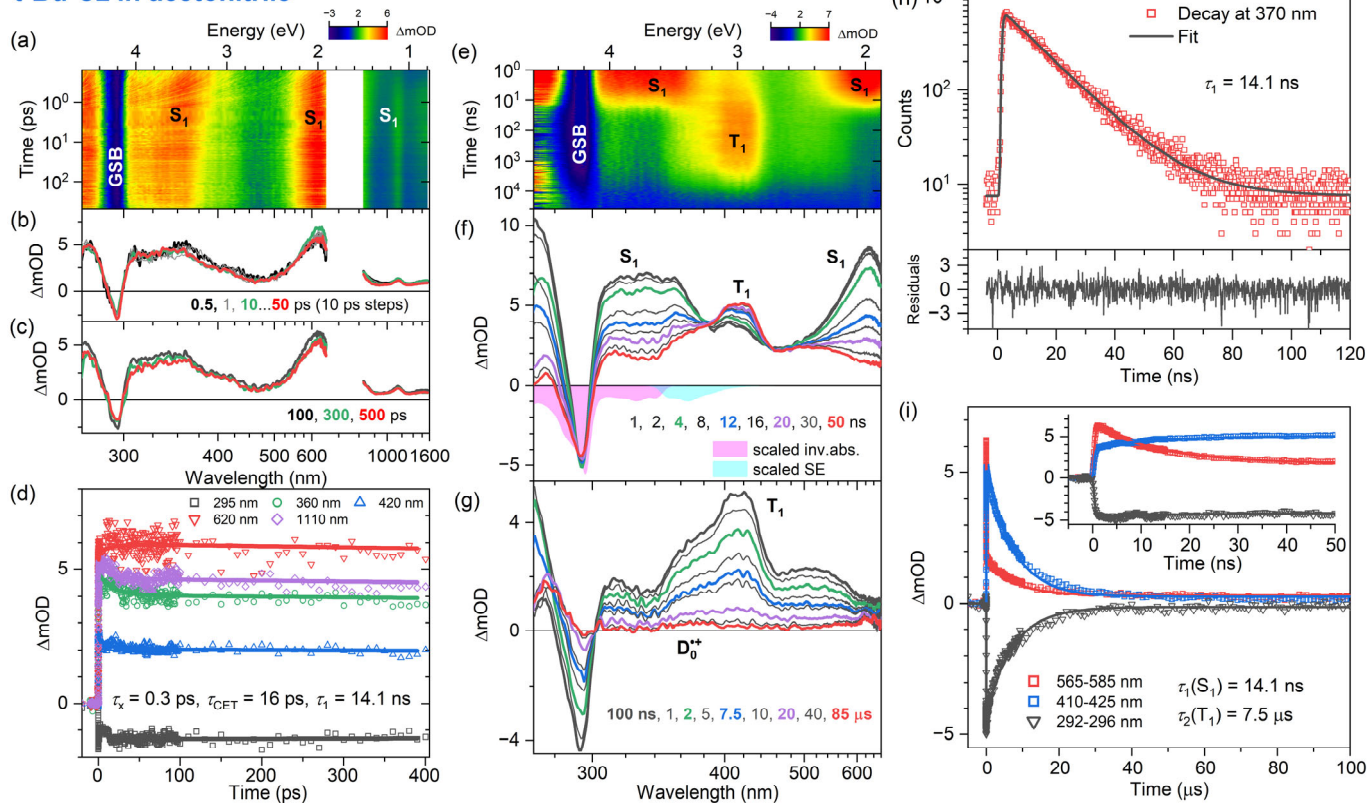
***t*-Bu-Cz in acetonitrile**

Figure 8. Same as Figure 6 but for the solvent acetonitrile.

4. Discussion

The electronic relaxation of Cz and *t*-Bu-Cz in organic solvents upon one-photon excitation in the deeper UV range below 300 nm is well described by a kinetic scheme involving S_x , S_1 and T_1 species. The initially populated S_x state has a (sub-)picosecond IC lifetime. The S_1 state shows characteristic ESA bands with peaks at 350, 600 and 1100 nm. The ESA band at 350 nm is reported here for the first time, and the same holds for a pronounced $S_0 \rightarrow S_2$ bleach band at 290 nm. The total lifetime of the S_1 state in deaerated solutions is in the range of 13–15 ns and only weakly dependent on the solvent. This result may be compared with previous time-resolved fluorescence experiments for Cz: For isolated jet-cooled carbazole molecules in the gas phase, a value of 29.4 ns for the $S_0 \rightarrow S_1$ (0–0) transition [19] located at 324.59 nm (3.8197 eV) [21] was found. Transient fluorescence studies in solution have reported total S_1 lifetimes in the range of 7–15 ns [17,26,29,32,33]. The S_1 lifetimes in the 13–15 ns range obtained for Cz and *t*-Bu-Cz are confirmed by the nanosecond transient absorption experiments which also provide clean spectral fingerprints of the T_1 state, with a peak absorption at 420 nm and a long absorption tail toward 600 nm. The T_1 state is populated from S_1 by ISC, and its lifetime for both carbazole derivatives is in the range of several microseconds. Based on the relative amplitudes of the S_1 and T_1 absorption in the ns-TA spectra and known absorption coefficients for the two states from the literature [54], we estimate a quantum yield for T_1 triplet formation of typically 51–56% for Cz and *t*-Bu-Cz in most of the solvents.

The lifetimes of the S_1 and T_1 states of Cz and *t*-Bu-Cz are very sensitive to the presence of $O_2(^3\Sigma_g^-)$ in the three organic solvents. We note that in another set of TCSPC and ns-TA experiments, we obtained S_1 lifetimes in the range of 6–8 ns in not fully deoxygenated solutions and also observed a drastic reduction of the T_1 lifetime from about 10 μ s down to 25–80 ns. Martin and Ware measured S_1 lifetimes of 14.8 and 8.0 ns for Cz in O_2 -free and aerated cyclohexane, respectively [26]. Similarly, Bonesi and Erra-Balsells obtained S_1 lifetimes of 14.2/8.70 ns in cyclohexane and 15.1/7.80 ns in acetonitrile under O_2 -free/aerated conditions [32].

Different S_1 quenching mechanisms of $O_2(^3\Sigma_g^-)$ need to be considered to understand this effect [58]: Quenching via the pathway $S_1 + O_2(^3\Sigma_g^-) \rightarrow T_1 + O_2(^1\Delta_g)$ requires an S_1 – T_1 energy gap of at least 0.98 eV [58] to generate $O_2(^1\Delta_g)$ and, therefore, cannot take place in Cz and *t*-Bu-Cz, because the S_1 – T_1 energy gap of Cz is 0.6 eV [17]. Viable pathways are the $O_2(^3\Sigma_g^-)$ -enhanced ISC process via $S_1 + O_2(^3\Sigma_g^-) \rightarrow T_1 + O_2(^3\Sigma_g^-)$ and also enhancement of the IC channel via $S_1 + O_2(^3\Sigma_g^-) \rightarrow S_0 + O_2(^3\Sigma_g^-)$. In addition, the deactivation channel $S_1 + O_2(^3\Sigma_g^-) \rightarrow T_2 + O_2(^3\Sigma_g^-)$ (with subsequent fast $T_2 \rightarrow T_1$ IC) [58] should be available in Cz and *t*-Bu-Cz [59].

Next, we consider quenching of the T_1 state by $O_2(^3\Sigma_g^-)$. Because the T_1 – S_0 energy gap of the two carbazoles is about 3.1 eV [17] and thus clearly larger than the 1.6 eV required for generating $O_2(^1\Sigma_g^+)$, quenching of the T_1 triplet state by $O_2(^3\Sigma_g^-)$ can occur via the three channels $T_1 + O_2(^3\Sigma_g^-) \rightarrow S_0 + O_2(^1\Sigma_g^+)$, $T_1 + O_2(^3\Sigma_g^-) \rightarrow S_0 + O_2(^1\Delta_g)$ and $T_1 + O_2(^3\Sigma_g^-) \rightarrow S_0 + O_2(^3\Sigma_g^-)$ [58]. For the T_1 state of Cz, Garner and Wilkinson reported a high $O_2(^3\Sigma_g^-)$ quenching rate constant of 5.7×10^9 L mol^{−1} s^{−1} in aerated benzene (for an O_2 concentration of 1.7×10^{-3} mol L^{−1}), which could arise from the influence of Cz charge transfer states [27]. In any case, the impact of $O_2(^3\Sigma_g^-)$ on the S_1 and T_1 lifetimes is substantial and needs to be carefully addressed in the TCSPC and ns-TA experiments. It also explains the spread of 7–15 ns in the S_1 lifetimes reported in the literature [17,26,29,32,33].

Furthermore, we note that we did not detect any steady-state phosphorescence from the T_1 state. In the literature, phosphorescence lifetimes in the range of 7.8–8.0 s have been measured for Cz in solid organic matrices only at a temperature of 77 K [17,22,32], with a phosphorescence quantum yield of 44% [17,32]. However, phosphorescence has so far not been observed at 300 K in organic solvents [60]. Assuming a temperature-independent radiative T_1 lifetime of 18 s [17,32] and taking our total T_1 lifetime of ca. 10 μ s from the ns-TA experiments, we estimate a phosphorescence quantum yield of 6×10^{-7} at 296 K, so

the phosphorescence will be very hard to detect, and the primary decay channel from T_1 is ISC.

Based on our femtosecond transient absorption data, we did not find clear indications for substantial ICT character of the S_1 state in Cz and *t*-Bu-Cz. The mirror-image-type structured absorption and emission spectra with small Stokes shifts support this interpretation, suggesting only minor structural and electronic changes in the S_1 state. We also did not find spectral evidence for the formation of carbazolyl radicals (Cz^\bullet), which were observed earlier by Hiyoshi et al. in their nanosecond transient absorption study [37]. However, in all of the solvents, we found spectral signatures for the formation of a small fraction of $Cz^{\bullet+}$ and *t*-Bu-Cz $^{\bullet+}$ radical cations, which show a broad absorption band spanning the wavelength range of 340–660 nm. They are generated by two-photon excitation induced by the pump laser.

The current results for “isolated” Cz and *t*-Bu-Cz molecules in organic solvents provide relevant photophysical and kinetic data for the interpretation of their electronic contributions in more complex environments, such as carbazole-based thin film materials or blue-emitting TADF compounds employing Cz-type derivatives as electron donor group [6,9,61,62], where competing channels, such as, for example, ICT processes, singlet–singlet, singlet–triplet and triplet–triplet annihilation take place simultaneously. For instance, the energetic position of the S_1 state of the Cz-type donor relative to the electronic states in the acceptor part of modern TADF dyes is relevant to the efficient transfer of the initial excitation to the acceptor. Moreover, the high-lying S_1 and T_1 states of carbazole-based host materials are of general importance for OLED operation, as the light-emitting states of the guest molecule are not subject to quenching by triplet energy transfer to the host.

Author Contributions: Conceptualization, K.O. and T.L.; methodology, K.O. and T.L.; investigation, K.M.K., D.G., K.O. and T.L.; writing—original draft preparation, K.O., T.L. and K.M.K.; writing—review and editing, K.O., T.L. and K.M.K.; supervision, K.O. and T.L. All authors have read and agreed to the published version of the manuscript.

Funding: This research received no external funding.

Data Availability Statement: Data are contained within the article.

Acknowledgments: We thank M. Dango for supporting K.M.K. and D.G. in the lab during this project.

Conflicts of Interest: The authors declare no conflicts of interest.

References

1. Blouin, N.; Leclerc, M. Poly(2,7-carbazole)s: Structure-Property Relationships. *Acc. Chem. Res.* **2008**, *41*, 1110–1119. [[CrossRef](#)]
2. Beaupré, S.; Leclerc, M. PCDTBT: En route for low cost plastic solar cells. *J. Mater. Chem. A* **2013**, *1*, 11097–11105. [[CrossRef](#)]
3. Shizu, K.; Lee, J.; Tanaka, H.; Nomura, H.; Yasuda, T.; Kaji, H.; Adachi, C. Highly efficient electroluminescence from purely organic donor–acceptor systems. *Pure Appl. Chem.* **2015**, *87*, 627–638. [[CrossRef](#)]
4. Dumur, F. Carbazole-based polymers as hosts for solution-processed organic light-emitting diodes: Simplicity, efficacy. *Org. Electron.* **2016**, *25*, 345–361. [[CrossRef](#)]
5. Ledwon, P. Recent advances of donor-acceptor type carbazole-based molecules for light emitting applications. *Org. Electron.* **2019**, *75*, 105422. [[CrossRef](#)]
6. Wex, B.; Kaafarani, B.R. Perspective on carbazole-based organic compounds as emitters and hosts in TADF applications. *J. Mater. Chem. C* **2017**, *5*, 8622–8653. [[CrossRef](#)]
7. Kondo, Y.; Yoshiura, K.; Kitera, S.; Nishi, H.; Oda, S.; Gotoh, H.; Sasada, Y.; Yanai, M.; Hatakeyama, T. Narrowband deep-blue organic light-emitting diode featuring an organoboron-based emitter. *Nat. Photonics* **2019**, *13*, 678–682. [[CrossRef](#)]
8. Ahn, D.H.; Kim, S.W.; Lee, H.; Ko, I.J.; Karthik, D.; Lee, J.Y.; Kwon, J.H. Highly efficient blue thermally activated delayed fluorescence emitters based on symmetrical and rigid oxygen-bridged boron acceptors. *Nat. Photonics* **2019**, *13*, 540–546. [[CrossRef](#)]

9. Hwang, J.; Koh, C.W.; Ha, J.M.; Woo, H.Y.; Park, S.; Cho, M.J.; Choi, D.H. Aryl-Annulated [3,2-*a*] Carbazole-Based Deep-Blue Soluble Emitters for High-Efficiency Solution-Processed Thermally Activated Delayed Fluorescence Organic Light-Emitting Diodes with CIE_y < 0.1. *ACS Appl. Mater. Interfaces* **2021**, *13*, 61454–61462. [[PubMed](#)]
10. Lee, H.; Braveenth, R.; Muruganatham, S.; Jeon, C.Y.; Lee, H.S.; Kwon, J.H. Efficient pure blue hyperfluorescence devices utilizing quadrupolar donor-acceptor-donor type of thermally activated delayed fluorescence sensitizers. *Nat. Commun.* **2023**, *14*, 419. [[CrossRef](#)]
11. Hofkens, J.; Cotlet, M.; Vosch, T.; Tinnefeld, P.; Weston, K.D.; Ego, C.; Grimsdale, A.; Müllen, K.; Beljonne, D.; Brédas, J.L.; et al. Revealing competitive Förster-type resonance energy-transfer pathways in single bichromophoric molecules. *Proc. Natl. Acad. Sci. USA* **2003**, *100*, 13146–13151. [[CrossRef](#)] [[PubMed](#)]
12. Ruseckas, A.; Ribierre, J.C.; Shaw, P.E.; Staton, S.V.; Burn, P.L.; Samuel, I.D.W. Singlet energy transfer and singlet-singlet annihilation in light-emitting blends of organic semiconductors. *Appl. Phys. Lett.* **2009**, *95*, 183305. [[CrossRef](#)]
13. Hedley, G.J.; Schröder, T.; Steiner, F.; Eder, T.; Hofmann, F.J.; Bange, S.; Laux, D.; Höger, S.; Tinnefeld, P.; Lupton, J.M.; et al. Picosecond time-resolved photon antibunching measures nanoscale exciton motion and the true number of chromophores. *Nat. Commun.* **2021**, *12*, 1327. [[CrossRef](#)] [[PubMed](#)]
14. Haase, N.; Danos, A.; Pflumm, C.; Stachelek, P.; Brütting, W.; Monkman, A.P. Are the rates of Dexter transfer in TADF hyperfluorescence systems optically accessible? *Mater. Horiz.* **2021**, *8*, 1805–1815. [[CrossRef](#)] [[PubMed](#)]
15. Morgenroth, M.; Lenzer, T.; Oum, K. Understanding Excited-State Relaxation in 1,3-Bis(*N*-carbazolyl)benzene, a Host Material for Organic Light-Emitting Diodes. *J. Phys. Chem. C* **2023**, *127*, 4582–4593. [[CrossRef](#)]
16. Walba, H.; Branch, G.E.K. The Absorption Spectra of Some *N*-Substituted *p*-Aminotriphenylmethyl Ions. *J. Am. Chem. Soc.* **1951**, *73*, 3341–3348. [[CrossRef](#)]
17. Adams, J.E.; Mantulin, W.W.; Huber, J.R. Effect of Molecular Geometry on Spin-Orbit Coupling of Aromatic Amines in Solution. Diphenylamine, Iminobenzyl, Acridan, and Carbazole. *J. Am. Chem. Soc.* **1973**, *95*, 5477–5481. [[CrossRef](#)]
18. Johnson, G.E. A Spectroscopic Study of Carbazole by Photoselection. *J. Phys. Chem.* **1974**, *78*, 1512–1521. [[CrossRef](#)]
19. Auty, A.R.; Jones, A.C.; Phillips, D. Spectroscopy and decay dynamics of jet-cooled carbazole and *N*-ethylcarbazole and their homocyclic analogues. *Chem. Phys.* **1976**, *103*, 163–182. [[CrossRef](#)]
20. Yu, H.; Zain, S.M.; Eigenbrot, I.V.; Phillips, D. Investigation of carbazole derivatives and their van der Waals complexes in the jet by laser-induced fluorescence spectroscopy. *J. Photochem. Photobiol. A* **1994**, *80*, 7–16. [[CrossRef](#)]
21. Yi, J.T.; Alvarez-Valtierra, L.; Pratt, D.W. Rotationally resolved S₁ ← S₀ electronic spectra of fluorene, carbazole, and dibenzofuran: Evidence for Herzberg-Teller coupling with the S₂ state. *J. Chem. Phys.* **2006**, *124*, 244302. [[CrossRef](#)] [[PubMed](#)]
22. Henry, B.R.; Kasha, M. Triplet-Triplet Absorption Studies on Aromatic and Heterocyclic Molecules at 77 °K. *J. Chem. Phys.* **1967**, *47*, 3319–3327. [[CrossRef](#)]
23. Fratev, F.; Hermann, H.; Olbrich, G.; Polansky, O.E. Höhere Triplettanregungszustände von Fluoren, Carbazol und Benzologen: CNDO-CI-Berechnungen und Triplett-Triplett-Absorptionsmessungen. *Z. Naturforsch. A Phys. Phys. Chem. Kosmophys.* **1976**, *31*, 84–86. [[CrossRef](#)]
24. Johnson, G.E. Intramolecular excimer formation in carbazole double molecules. *J. Chem. Phys.* **1974**, *61*, 3002–3008. [[CrossRef](#)]
25. Masuhara, H.; Tohgo, Y.; Mataga, N. Fluorescence quenching processes of carbazole-amine systems as revealed by laser photolysis method. *Chem. Lett.* **1975**, *4*, 59–62. [[CrossRef](#)]
26. Martin, M.M.; Ware, W.R. Fluorescence Quenching of Carbazole by Pyridine and Substituted Pyridines. Radiationless Processes in the Carbazole-Amine Hydrogen Bonded Complex. *J. Phys. Chem.* **1978**, *82*, 2770–2776. [[CrossRef](#)]
27. Garner, A.; Wilkinson, F. Quenching of triplet states by molecular oxygen and the role of charge-transfer interactions. *Chem. Phys. Lett.* **1977**, *45*, 432–435. [[CrossRef](#)]
28. Bigelow, R.W.; Ceasar, G.P. Hydrogen Bonding and *N*-Alkylation Effects on the Electronic Structure of Carbazole. *J. Phys. Chem.* **1979**, *83*, 1790–1795. [[CrossRef](#)]
29. Johnson, G.E. Fluorescence Quenching of Carbazoles. *J. Phys. Chem.* **1980**, *84*, 2940–2946. [[CrossRef](#)]
30. Martin, M.M.; Bréhéret, E. Hydrogen Bonding Interaction Effect on Carbazole Triplet State Photophysics. *J. Phys. Chem.* **1982**, *86*, 107–111. [[CrossRef](#)]
31. Kikuchi, K.; Yamamoto, S.A.; Kokubun, H. Hydrogen atom transfer reaction from excited carbazole to pyridine. *J. Photochem.* **1984**, *24*, 271–283. [[CrossRef](#)]
32. Bonesi, S.M.; Erra-Balsells, R. Electronic spectroscopy of carbazole and *N*- and *C*-substituted carbazoles in homogeneous media and in solid matrix. *J. Lumin.* **2001**, *93*, 51–74. [[CrossRef](#)]
33. Boo, B.H.; Ryu, S.Y.; Kang, H.S.; Koh, S.G.; Park, C.-J. Time-resolved Fluorescence Studies of Carbazole and Poly(*N*-vinylcarbazole) for Elucidating Intramolecular Excimer Formation. *Bull. Korean Chem. Soc.* **2010**, *57*, 406–411. [[CrossRef](#)]
34. Bayda-Smykaj, M.; Burdzinski, G.; Ludwiczak, M.; Hug, G.L.; Marciniak, B. Early Events in the Photoinduced Electron Transfer between Carbazole and Divinylbenzene in a Silylene-Bridged Donor-Acceptor Compound. *J. Phys. Chem. C* **2020**, *124*, 19522–19529. [[CrossRef](#)]

35. Thornton, G.L.; Phelps, R.; Orr-Ewing, A.J. Transient absorption spectroscopy of the electron transfer step in the photochemically activated polymerizations of *N*-ethylcarbazole and 9-phenylcarbazole. *Phys. Chem. Chem. Phys.* **2021**, *23*, 18378–18392. [[CrossRef](#)] [[PubMed](#)]
36. Yang, Y.; Jiang, Z.; Liu, Y.; Guan, T.; Zhang, Q.; Qin, C.; Jiang, K.; Liu, Y. Transient Absorption Spectroscopy of a Carbazole-Based Room-Temperature Phosphorescent Molecule: Real-Time Monitoring of Singlet-Triplet Transitions. *J. Phys. Chem. Lett.* **2022**, *13*, 9381–9389. [[CrossRef](#)] [[PubMed](#)]
37. Hiyoshi, R.; Hiura, H.; Sakamoto, Y.; Mizuno, M.; Sakai, M.; Takahashi, H. Time-resolved absorption and time-resolved Raman spectroscopies of the photochemistry of carbazole and *N*-ethylcarbazole. *J. Mol. Struct.* **2003**, *661–662*, 481–489. [[CrossRef](#)]
38. Notsuka, N.; Nakanotani, H.; Noda, H.; Goushi, K.; Adachi, C. Observation of Nonradiative Deactivation Behavior from Singlet and Triplet States of Thermally Activated Delayed Fluorescence Emitters in Solution. *J. Phys. Chem. Lett.* **2020**, *11*, 562–566. [[CrossRef](#)] [[PubMed](#)]
39. Kim, H.J.; Kang, H.; Jeong, J.-E.; Park, S.H.; Koh, C.W.; Kim, C.W.; Woo, H.Y.; Cho, M.J.; Park, S.; Choi, D.H. Ultra-Deep-Blue Aggregation-Induced Delayed Fluorescence Emitters: Achieving Nearly 16% EQE in Solution-Processed Nondoped and Doped OLEDs with $CIE_y < 0.1$. *Adv. Funct. Mater.* **2021**, *31*, 2102588.
40. Morgenroth, M.; Scholz, M.; Guy, L.; Oum, K.; Lenzer, T. Spatiotemporal Mapping of Efficient Chiral Induction by Helicene-Type Additives in Copolymer Thin Films. *Angew. Chem. Int. Ed.* **2022**, *61*, e202203075. [[CrossRef](#)]
41. Oum, K.; Lenzer, T.; Scholz, M.; Jung, D.Y.; Sul, O.; Cho, B.J.; Lange, J.; Müller, A. Observation of Ultrafast Carrier Dynamics and Phonon Relaxation of Graphene from the Deep-Ultraviolet to the Visible Region. *J. Phys. Chem. C* **2014**, *118*, 6454–6461. [[CrossRef](#)]
42. Flender, O.; Scholz, M.; Klein, J.R.; Oum, K.; Lenzer, T. Excited-state relaxation of the solar cell dye D49 in organic solvents and on mesoporous Al₂O₃ and TiO₂ thin films. *Phys. Chem. Chem. Phys.* **2016**, *18*, 26010–26019. [[CrossRef](#)]
43. Dobryakov, A.L.; Kovalenko, S.A.; Weigel, A.; Pérez Lustres, J.L.; Lange, J.; Müller, A.; Ernsting, N.P. Femtosecond pump/supercontinuum-probe spectroscopy: Optimized setup and signal analysis for single-shot spectral referencing. *Rev. Sci. Instrum.* **2010**, *81*, 113106. [[CrossRef](#)] [[PubMed](#)]
44. Merker, A.; Scholz, M.; Morgenroth, M.; Lenzer, T.; Oum, K. Photoinduced Dynamics of (CH₃NH₃)₄Cu₂Br₆ Thin Films Indicating Efficient Triplet Photoluminescence. *J. Phys. Chem. Lett.* **2021**, *12*, 2736–2741. [[CrossRef](#)] [[PubMed](#)]
45. Ljubić, I.; Sabljčić, A. CASSCF/CASPT2 and TD-DFT Study of Valence and Rydberg Electronic Transitions in Fluorene, Carbazole, Dibenzofuran, and Dibenzothiophene. *J. Phys. Chem. A* **2011**, *115*, 4840–4850. [[CrossRef](#)] [[PubMed](#)]
46. Platt, J.R. Classification of Spectra of Cata-Condensed Hydrocarbons. *J. Chem. Phys.* **1949**, *17*, 484–495. [[CrossRef](#)]
47. Lohse, P.W.; Bürsing, R.; Lenzer, T.; Oum, K. Exploring 12'-Apo-β-carotenoic-12'-acid as an Ultrafast Polarity Probe for Ionic Liquids. *J. Phys. Chem. B* **2008**, *112*, 3048–3057. [[CrossRef](#)]
48. Lide, D.R. (Ed.) *Handbook of Chemistry and Physics*, 85th ed.; CRC Press: Boca Raton, FL, USA, 2004.
49. Schwarzer, D.; Troe, J.; Votsmeier, M.; Zerezke, M. Collisional deactivation of vibrationally highly excited azulene in compressed liquids and supercritical fluids. *J. Chem. Phys.* **1996**, *105*, 3121–3131. [[CrossRef](#)]
50. Schwarzer, D.; Hanisch, C.; Kutne, P.; Troe, J. Vibrational Energy Transfer in Highly Excited Bridged Azulene-Aryl Compounds: Direct Observation of Energy Flow through Aliphatic Chains and into the Solvent. *J. Phys. Chem. A* **2002**, *106*, 8019–8028. [[CrossRef](#)]
51. Kovalenko, S.A.; Schanz, R.; Hennig, H.; Ernsting, N.P. Cooling dynamics of an optically excited molecular probe in solution from femtosecond broadband absorption spectroscopy. *J. Chem. Phys.* **2001**, *115*, 3256–3273. [[CrossRef](#)]
52. Andersson, P.O.; Gillbro, T. Photophysics and dynamics of the lowest excited singlet state in long substituted polyenes with implications to the very long-chain limit. *J. Chem. Phys.* **1995**, *103*, 2509–2519. [[CrossRef](#)]
53. Lenzer, T.; Ehlers, F.; Scholz, M.; Oswald, R.; Oum, K. Assignment of carotene S* state features to the vibrationally hot ground electronic state. *Phys. Chem. Chem. Phys.* **2010**, *12*, 8832–8839. [[CrossRef](#)] [[PubMed](#)]
54. Martin, M.; Bréhéret, E.; Tifibel, F.; Lacourbas, B. Two-Photon Stepwise Dissociation of Carbazole in Solution. *J. Phys. Chem.* **1980**, *84*, 70–72. [[CrossRef](#)]
55. Shida, T.; Nosaka, Y.; Kato, T. Electronic Absorption Spectra of Some Cation Radicals as Compared with Ultraviolet Photoelectron Spectra. *J. Phys. Chem.* **1978**, *82*, 695–698. [[CrossRef](#)]
56. Haink, H.J.; Adams, J.E.; Huber, J.R. The Electronic Structure of Aromatic Amines: Photoelectron Spectroscopy of Diphenylamine, Iminobenzyl, Acridan and Carbazole. *Ber. Bunsenges. Phys. Chem.* **1974**, *78*, 436–440. [[CrossRef](#)]
57. Liptay, W. Electrochromism and Solvatochromism. *Angew. Chem. Int. Ed.* **1967**, *8*, 177–188. [[CrossRef](#)]
58. Schweitzer, C.; Schmidt, R. Physical Mechanisms of Generation and Deactivation of Singlet Oxygen. *Chem. Rev.* **2003**, *103*, 1685–1757. [[CrossRef](#)] [[PubMed](#)]
59. Hernández, F.J.; Crespo-Otero, R. Excited state mechanisms in crystalline carbazole: The role of aggregation and isomeric defects. *J. Mater. Chem. C* **2021**, *9*, 11882–11892. [[CrossRef](#)]
60. Chen, C.; Chong, K.C.; Pan, Y.; Qi, G.; Xu, S.; Liu, B. Revisiting Carbazole: Origin, Impurity, and Properties. *ACS Mater. Lett.* **2021**, *3*, 1081–1087. [[CrossRef](#)]

61. Hosokai, T.; Matsuzaki, H.; Nakanotani, H.; Tokumaru, K.; Tsutsui, T.; Furube, A.; Nasu, K.; Nomura, H.; Yahiro, M.; Adachi, C. Evidence and mechanism of efficient thermally activated delayed fluorescence promoted by delocalized excited states. *Sci. Adv.* **2017**, *3*, e1603282. [[CrossRef](#)]
62. Godumala, M.; Choi, S.; Cho, M.J.; Choi, D.H. Recent breakthroughs in thermally activated delayed fluorescence organic light emitting diodes containing non-doped emitting layers. *J. Mater. Chem. C* **2019**, *7*, 2172–2198. [[CrossRef](#)]

Disclaimer/Publisher’s Note: The statements, opinions and data contained in all publications are solely those of the individual author(s) and contributor(s) and not of MDPI and/or the editor(s). MDPI and/or the editor(s) disclaim responsibility for any injury to people or property resulting from any ideas, methods, instructions or products referred to in the content.